



CHORUS

This is the accepted manuscript made available via CHORUS. The article has been published as:

Fast Ion Transport in the Three-Dimensional Reversed-Field Pinch

P. J. Bonfiglio, J. K. Anderson, J. Boguski, J. Kim, J. Egedal, M. Gobbin, D. A. Spong, and E. Parke

Phys. Rev. Lett. **123**, 055001 — Published 29 July 2019

DOI: [10.1103/PhysRevLett.123.055001](https://doi.org/10.1103/PhysRevLett.123.055001)

Fast Ion Transport in the Three-Dimensional Reversed-Field Pinch

P. J. Bonfiglio,* J. K. Anderson, J. Boguski, J. Kim, and J. Egedal
University of Wisconsin - Madison, Madison, WI 53706, USA

M. Gobbin
Consorzio RFX, Associazione Euratom-ENEA sulla Fusione, Padova 35127, Italy

D. A. Spong
Oak Ridge National Laboratory, Oak Ridge, TN 37831, USA

E. Parke
TAE Technologies Inc., Foothill Ranch, CA 92610, USA
(Dated: June 27, 2019)

We report on the first comprehensive experimental and numerical study of fast ion transport in the helical reversed-field pinch. Classical orbit effects dominate the macroscopic confinement properties. The strongest effect arises from growth in the dominant fast ion guiding-center island, but substantial influence from remnant subdominant tearing modes also plays a critical role. At the formation of the helical RFP, neutron flux measurements indicate a drastic loss of fast ions at sufficient subdominant mode amplitudes. Simulations corroborate these measurements and suggest subdominant tearing modes strongly limit fast ion behavior. Previous work details a sharp thermal transport barrier and suggests the helical RFP as an ohmically heated fusion reactor candidate; the enhanced transport of fast ions reported here identifies a key challenge for this scheme but a workable scenario is conceivable with low subdominant tearing mode amplitudes.

The reversed-field pinch (RFP) provides a unique environment to study fast ion confinement and transport in both axisymmetric and helical geometries. RFP plasmas normally possess a broad toroidal n -number spectrum of long wavelength tearing modes characterized mostly by the $m = 1$ poloidal mode number. This standard RFP mode configuration may be called the multiple helicity (MH) state. A quasi-single helical (QSH) state forms when the MH state condenses down to a spectrum dominated by a single $m = 1$ mode. The nonlinear coupling between tearing modes breaks, or weakens, and allows for the core-resonant mode to saturate at large amplitude.[1–3] Observations show that at adequately high Lundquist number, $S = \frac{Lv_A}{\eta} \sim \frac{I_p T_e^{3/2}}{\sqrt{n_e}} \sim 10^6$, the innermost-resonant tearing mode grows and envelops the magnetic axis while the subdominant modes maintain, or decrease, their amplitudes.[4] This establishes a helical equilibrium with periodicity defined by the core-resonant mode. The

spectral index, $N_s = \left[\sum_n \left(\frac{\tilde{b}_n^2}{\sum_n \tilde{b}_n^2} \right)^2 \right]^{-1}$, provides a parameter to help define this state, where \tilde{b}_n denotes the tearing mode amplitudes and $N_s \lesssim 1.2$ represents the QSH state.

This new, self-organized helical state creates strong thermal transport barriers, making it a possible scenario for a low-magnetic-field ohmic fusion reactor.[5–9] Burning plasmas, however, require good confinement of energetic alpha particles. Therefore, the behavior of fast ions in the QSH state poses a critical question for the helical RFPs fusion relevance and mandates a comprehensive

experimental and computational investigation.

A tangentially oriented neutral beam injector (NBI) produces core-localized, high-pitch, 25 keV hydrogen or deuterium ions for analysis in the Madison Symmetric Torus (MST). Neutral beam born ions on MST, analogous to alpha particles in a reactor, act as a testbed for energetic particle physics in the QSH state.[10] In comparison, NBI born ions have a similar gyroradius relative to device size ($\rho_{fi}/a \sim 0.1$), superthermal speed ($v_{fi}/v_{th} \sim 13$), and superalfvénic speed ($v_{fi}/v_A > 1$) but possess a localized pitch-angle distribution due to injection geometry while alpha particles form an isotropic distribution.[11] MST ($R_0 = 1.5$ m, $a = 0.5$ m) produces deuterium RFP plasmas with total current $I_p = 200–600$ kA which both heats the plasma and generates the confining field with central strength $|B(0)| = 0.2–0.5$ T and electron temperature $T_e(0) = 200–2000$ eV. Typically, MST plasmas transition to the QSH state in non-reversed plasmas ($q(a) = 0$) at moderate I_p (> 350 kA) and low density ($\bar{n}_e < 0.5 \times 10^{13}$ cm $^{-3}$) with an $m = 1$, $n = 5$ dominant perturbation. Depending on plasma conditions, the QSH state in MST saturates at $\frac{b_5}{|B(a)|} \sim 5–8\%$ with subdominant mode amplitudes totaling around 0.5–2%.

One may expect that this helical perturbation will bear similar complications of symmetry breaking common in unoptimized stellarators or discrete-coil-induced tokamak field ripples and result in strong radial transport.[12–17] However, prior numerical studies show that the large non-axisymmetric magnetic perturbation characterizing the QSH state does not induce unoptimized stellarator-like losses for thermal particles.[18]

Only at experimentally unattainable perturbation levels can the helically trapped superbanana orbits appreciably contribute to thermal transport.[19]

This letter presents an experimental and computational examination of fast ion confinement and transport in the RFP QSH state. In the MH state, fast ions ignore the magnetic stochasticity induced by the tearing modes and achieve classical confinement.[20] In the five-fold periodic QSH state in MST, there is a substantial reduction in fast ion confinement. Tearing modes create a stochastic fast ion phase-space capable of producing the observed particle losses. While the $n = 5$ helical perturbation breaks toroidal symmetry, fast ions largely ignore the superbanana regime of neoclassical transport.[21] Fast ion losses due to energetic particle driven Alfvénic instabilities are also negligible in the QSH state and are considered in more detail in [21].

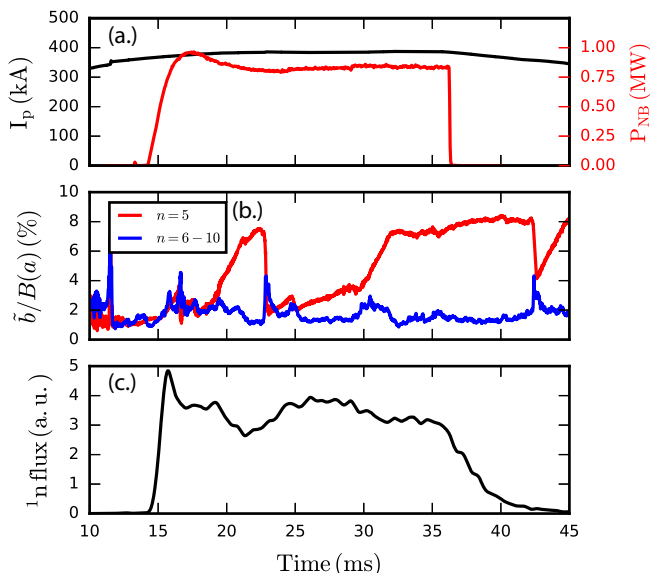


FIG. 1. A representative QSH discharge in MST. (a.) Plasma current and neutral beam power (b.) Normalized tearing mode amplitudes for the dominant ($n = 5$) and subdominant ($n = 6 - 10$) modes from edge magnetic coils (c.) Global neutron flux from D-D fusion events.

Measurements of the rate of D-D fusion reactions provide a measure of the fast ion population in MST since the neutron flux is proportional to the fast ion density and the thermal deuterium population is kept relatively fixed by gas puffing. Figure 1 is a typical QSH discharge studied on MST. NBI is applied during the current flat top, (a.), while the magnetic mode amplitudes, (b.), show multiple transitions (21-23; 30-42 ms) into and out of the QSH state. The response of the global neutron flux, (c.), is affected by both the dominant and subdominant tearing amplitudes. In order to examine this response more thoroughly, neutron measurements were ensembled across hundreds of discharges as a function of tearing mode amplitudes.

The time domain for a given discharge with deuterium NBI was split into 250 μs windows during the beam injection. For each time window, the tearing mode amplitudes were found from edge magnetic coils and averaged to single values for the dominant ($n = 5$) and summed subdominant ($n = 6 - 10$) modes. The rate of change of the neutron flux was then calculated for each window, normalized to the window center, and binned according to the respective tearing mode amplitudes. This process was repeated across similar QSH plasmas with varied helical perturbation strengths and averaged together to produce Figure 2 (a.). Part (b.) is the normalized rate of change shown in (a.) at two fixed core-resonant amplitudes: 1.7% and 6.7%. It is important to note that while the strength of the helical perturbation is experimentally controlled by altering the plasma current across fixed density, the subdominant modes possess no control mechanism. The change in the neutron flux is in response to the dynamically evolving tearing modes throughout the QSH transition.[22] Examining part (a.), the fast ion

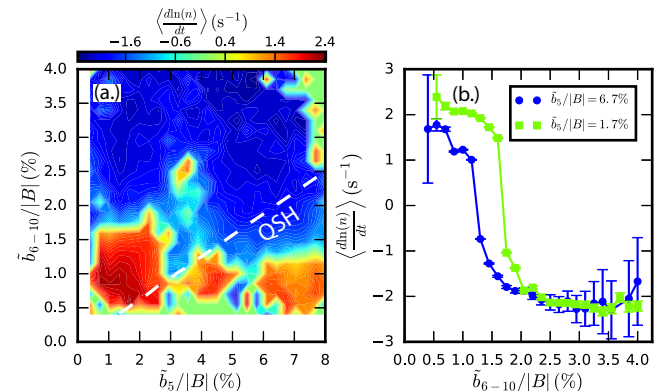


FIG. 2. (a.) Ensemble average of the normalized rate of change of the global neutron flux with the dashed area representing the QSH regime of $N_s < 1.2$ (b.) Line cuts of the ensembled neutron flux rate as a function of normalized subdominant tearing mode amplitude.

driven neutron flux decreases with fixed, low, subdominant mode amplitude and increasing $n = 5$ amplitude. Additionally, part (b.) shows that the neutron flux decreases more rapidly in the presence of stronger subdominant tearing modes in the QSH regime than in the MH regime. Figure 2 indicates an extremely sensitive coupling between dominant and subdominant modes affecting the global fast ion confinement. Upon closer inspection, the fast ion content in the QSH region appears to grow at low subdominant amplitudes (0.5-1.25%), which is closer to a purely helical state, and shrink with more modest amplitudes ($\tilde{b}_{6-10}/|B| > 1.25\%$).

Direct measurement of the global fast ion confinement time confirms drastic fast ion losses during the transition to the QSH state, contrary to confinement in the standard RFP. The fast ion confinement time, τ_{fi} , was mea-

sured on MST with the beam-blip technique [23], via the associated neutron flux decay, for ~ 500 QSH discharges of similar plasma conditions and varied helical perturbation strengths. The results are plotted as a function of normalized core-resonant amplitude in Figure 3 (a.). The data points were selected based upon favorable experimental conditions with reasonable error stemming from Thomson scattering electron temperature measurements. The dynamic nature of the subdominant mode amplitudes across the relatively large time-averaging window used for the beam-blip calculation produces larger subdominant mode amplitudes than that capable of being measured from the instantaneous neutron flux shown in Figure 2 (a.). Therefore, the weakened confinement results at high $n = 5$ amplitude are consistent with the blueish zone within the QSH region of Figure 2 (a.).

Fast ion loss times found from the Hamiltonian guiding-center particle tracking code ORBIT [24] are also plotted in Figure 3 (b.)-(d.). The ORBIT simulated loss times were calculated by depositing 600 fast ions in the plasma core with random pitch (v_{\parallel}/v) from 0 to 1. A particle was considered lost when it reached the wall boundary at which point its lost time was recorded.[25] The loss times were calculated as the mean of all the individual particles' lost times and plotted as a function of varied tearing mode amplitudes. The simulations included both pitch-angle and slowing collisions where the thermalization time for a 25 keV ion in typical MST plasma parameters is ~ 20 ms.[20] Each point corresponds to an average of 25 ORBIT simulations at particular tearing mode strengths with all other plasma parameters held constant.

The simulated fast ion loss times corroborate the experimental measurements and show a marked decrease in confinement in the transition from a MH to QSH state. Figure 3 (b.) replicates the experimental conditions as close as possible within ORBIT parameters and shows agreement with subplot (a.). Figure 3 (c.) plots τ_{fi} under the same constraints but with only the dominant $m = 1, n = 5$ mode active. Compared to the previous case with all tearing modes present, the simulated fast ion confinement drastically improves when only in the presence of the $n = 5$ mode. This indicates that the subdominant modes are instrumental in decreasing fast ion confinement and transport in the QSH state. Part (d.) of Figure 3 presents τ_{fi} as a function of scaled subdominant mode amplitudes at a fixed normalized core-resonant amplitude of 7%. This represents a transition from the far right of subplot (c.) to the far right of subplot (b.). The rapid convergence to QSH-like loss times demonstrates that even the slightest presence of subdominant tearing modes ($\sim 30\%$ of their typical time-averaged experimental values) leads to drastic fast ion losses. The simulations replicate the subdominant mode sensitivity within the QSH state present in the neutron measurements of Figure 2 that portrays regions of good and poor fast ion

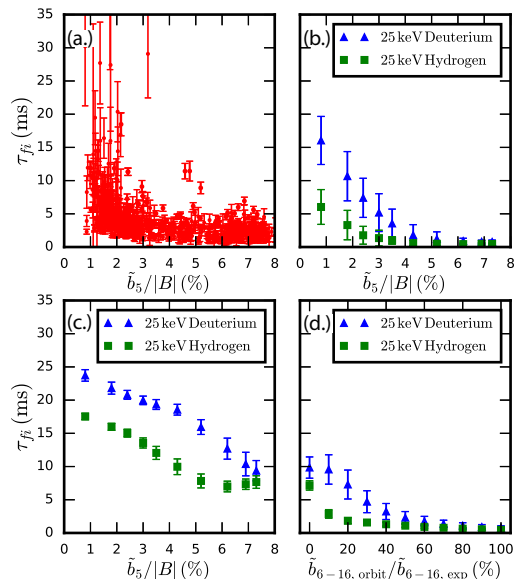


FIG. 3. (a.) Experimental τ_{fi} measured via beam-blip technique on MST (b.) Simulated τ_{fi} from ORBIT with $m = 1, n = 5 - 16$ and $m = 0, n = 1 - 4$ modes active (c.) Simulated τ_{fi} from ORBIT simulations with only the $m = 1, n = 5$ mode active (d.) Simulated τ_{fi} as a function of scaled subdominant mode amplitudes from ORBIT simulations with $\tilde{b}_5/|B| \approx 7\%$.

confinement sensitive to the remnant tearing modes.

The tearing mode closest to the core clearly shows confinement-reducing phase-space structures in ORBIT simulations. Figure 4 presents toroidally projected 25 keV deuterium Poincaré-puncture plots with increasing core-tearing amplitude in parts (a.)-(c.). The plots are toroidal projections across the toroidal angle, ζ , and the poloidal flux, ψ_p which acts as the radial coordinate. Part (d.) shows the fast ion structure associated with only the $n = 5$ mode active at high perturbation level. The well-defined nested surfaces near the plasma core in part (a.) demonstrate the well-confined nature of fast ions in the MH state.[20] As the helical perturbation strength grows in parts (b.) and (c.), however, those well-defined surfaces erode and the fast ion phase-space becomes more stochastic. The $n = 5$ fast ion guiding-center island [20] presents itself in the plots as the localized structure around $\psi_p \sim 0.6$. One can see that the associated island width grows with the helical perturbation strength. Part (d.) is the Poincaré plot produced in the same scenario as (c.) but all of the subdominant tearing modes have been removed, allowing a full view of the $n = 5$ island structure which spans a relatively large radial width that extends to the core region. This destroys the well ordered surfaces in part (a.) and allows fast ions in the core to quickly wander radially outward within the $n = 5$ island. The subdominant modes occur at large radii which, when coupled with the $n = 5$ island, result in significant island overlap and the observed stochasticity.

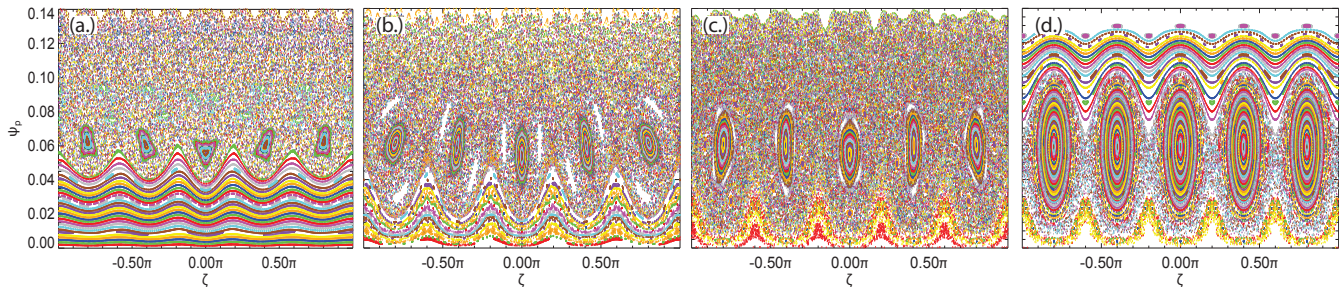


FIG. 4. ORBIT produced fast ion phase-space Poincaré-puncture plots projected onto the toroidal plane for 25 keV deuterium ions. Subplots (a.) - (c.) have normalized core-resonant tearing strengths of 0.8%, 4.6%, and 7.5% and experimental-like subdominant mode amplitudes. Subplot (d.) is the same as plot (c.) with the exclusion of all subdominant tearing modes.

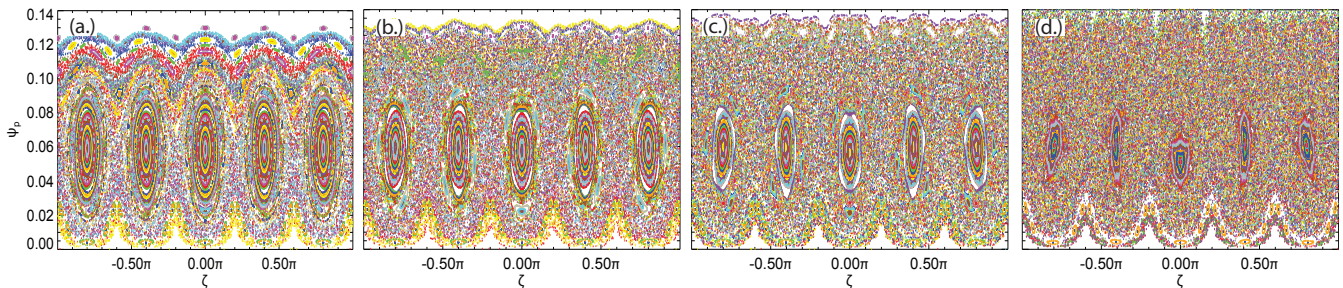


FIG. 5. ORBIT produced fast ion phase-space Poincaré-puncture plots projected onto the toroidal plane for 25 keV deuterium ions. The subplots (a.) - (d.), respectively, have scaled subdominant mode amplitudes of 10%, 30%, 60%, and 200% relative to their original value of $\bar{b}_{6-16}/|B| \sim 1.8\%$. All cases have a fixed normalized core-resonant tearing strength of 7.5% (same as Figure 4 (c.) and (d.)).

The deleterious effect of subdominant modes on the fast ion guiding-center phase-space is illustrated in Figure 5 for a QSH state ($\bar{b}_5/|B| = 7.5\%$) but with scaled subdominant mode amplitudes. Parts (a.) - (c.) of Figure 5 have weakened subdominant amplitudes relative to Figure 4 (c.). This allows for less island overlap, a larger $n = 5$ island, and a slightly improved confinement consistent with the simulations and neutron measurements. Part (d.) of Figure 5 has much larger subdominant amplitudes relative to Figure 4 (c.). In this case, the $n = 5$ island has shrunk considerably and almost all of the phase-space has become stochastic. A large $n = 5$ amplitude coupled with large subdominant amplitudes is extremely detrimental to fast ion confinement in the RFP while weaker subdominant modes result in a reduction of transport. Overall, in the QSH state, the large $n = 5$ guiding-center island transports core-localized particles radially outward where subdominant modes may greatly enhance the transport due to their significant overlap near the edge.

In summary, measurements of D-D fusion neutron flux show a strong response in the fast ion confinement as the RFP transitions from MH to QSH. These observations break from those of thermal particles where a sharp internal transport barrier can accompany QSH. ORBIT simulations confirm the dominant fast ion transport mecha-

nism is a developed stochasticity in the fast ion guiding-center phase-space, due to the increase in $n = 5$ amplitude, and is sharply impacted by the amplitude of remnant subdominant modes.

The critical importance of subdominant mode amplitude on fast ion confinement presents an obstacle for the idea of a helical RFP reactor. The NBI-born fast ions in MST have normalized parameters designed to mimic fast alphas in an envisioned reactor and the measured confinement is well below that required for a self-heated burning plasma. The experiment, though, is conducted at $S < 10^7$ which is more than 3 orders below that of a reactor. The most complete study of QSH mode scaling to date from the RFX-Mod device covers slightly more than one order of magnitude in S ($10^6 - 10^7$) [9, 26] and shows a favorable trend: the normalized strength of the dominant helical mode grows modestly while the subdominant modes drop by approximately a factor of 2. Should the trend continue to reactor-level Lundquist number, the fast ion phase-space will be nearly free of subdominant mode-induced orbit losses and result in reduced transport similar to that observed in the bottom-right of Figure 2 (a.). With well confined fast ions, the possibility of Alfvénic mode induced resonant transport may become an important factor (negligible in the NBI-heated MST case due to other dominant loss mechanisms [21, 22]).

Evaluation of fast ion confinement will be a critical mission of any next-step RFP experiment.

This work is supported by the U.S. DOE Office of Science, Office of Fusion Energy Sciences program under Award Number DE-FC02-05ER54814 and accomplished with the use of the infrastructure of Complex DOL (Budker Institute of Nuclear Physics, Russia). See Supplemental Material at for raw figure data shown in this letter.

* bonofiglo@wisc.edu

- [1] S. Assadi, S. C. Prager, and K. L. Sidikman, Phys. Rev. Lett. **69**, 281 (1992).
- [2] J. S. Sarff, S. Assadi, A. F. Almagri, M. Cekic, D. J. Den Hartog, G. Fiksel, S. A. Hokin, H. Ji, S. C. Prager, W. Shen, K. L. Sidikman, and M. R. Stoneking, Phys. Fluids B **5**, 2540 (1993).
- [3] P. Martin, A. Buffa, S. Cappello, F. D'Angelo, D. F. Escande, P. Franz, L. Marrelli, E. Martines, S. Ortolani, G. Spizzo, *et al.*, Phys. Plasmas **7**, 1984 (2005).
- [4] B. E. Chapman, F. Auriemma, W. Bergerson, D. Brower, S. Cappello, D. J. Den Hartog, W. Ding, P. Franz, S. Kumar, P. Innocente, *et al.*, "Direct diagnosis and parametric dependence of 3D helical equilibrium in the MST RFP," in *EX/P6-01 Proceedings of IAEA Conference* (2012).
- [5] I. Predebon, L. Marrelli, R. B. White, and P. Martin, Phys. Rev. Lett. **93**, 0145001 (2004).
- [6] R. Lorenzini, D. Terranova, A. Alfier, P. Innocente, E. Martines, R. Pasqualotto, and P. Zanca, Phys. Rev. Lett. **101**, 025005 (2008).
- [7] M. Gobbin, D. Bonfiglio, D. F. Escande, A. Fassina, L. Marrelli, A. Alfier, E. Martines, B. Momo, and D. Terranova, Phys. Rev. Lett. **106**, 025001 (2011).
- [8] R. Lorenzini, F. Auriemma, A. Fassina, E. Martines, D. Terranova, and F. Sattin, Phys. Rev. Lett. **116**, 185002 (2016).
- [9] R. Lorenzini *et al.*, Nature Physics **5**, 8 (2009).
- [10] J. K. Anderson, W. Capecchi, S. Eilerman, J. J. Kollner, M. D. Nornberg, J. A. Reusch, J. S. Sarff, and L. Lin, Plasma Phys. Control Fusion **56**, 094006 (2014).
- [11] David Hill (Chair) and Richard Hazeltine (Vice Chair), "Report of the FESAC Toroidal Alternates Panel," http://fusion.gat.com/tap/final_report.php/ (2008).
- [12] W. W. Heidbrink and G. J. Sadler, Nucl. Fusion **34**, 535 (1994).
- [13] R. B. White, R. J. Goldston, M. H. Redi, and R. V. Budny, Phys. Plasmas **3**, 3043 (1996).
- [14] M. H. Redi, H. E. Mynick, M. Siewattana, R. B. White, and M. C. Zarnstorff, Phys. Plasmas **6**, 3509 (1999).
- [15] H. E. Mynick, Phys. Plasmas **13**, 058102 (2006).
- [16] D. A. Spong, Phys. Plasmas **18**, 0656109 (2011).
- [17] D. A. Spong, Phys. Plasmas **22**, 055602 (2015).
- [18] M. Gobbin, G. Spizzo, L. Marrelli, and R. B. White, Phys. Rev. Lett. **105**, 195006 (2010).
- [19] J. A. Derr and J. L. Shohet, Phys. Rev. Lett. **43**, 1730 (1979).
- [20] G. Fiksel, B. Hudson, D. J. Den Hartog, R. M. Magee, R. O'Connell, S. C. Prager, A. D. Beklemishev, V. I. Davydenko, A. A. Ivanov, and Y. A. Tsidulko, Phys. Rev. Lett. **95**, 125001 (2005).
- [21] P. J. Bonofiglo, J. K. Anderson, M. Gobbin, D. A. Spong, J. Boguski, E. Parke, J. Kim, and J. Egedal, Phys. Plasmas **26**, 022502 (2019).
- [22] W. Capecchi, J. K. Anderson, P. J. Bonofiglo, J. Kim, R. M. Magee, R. McConnell, E. Parke, J. S. Sarff, and K. J. McCollam, Nucl. Fusion (2019), <https://doi.org/10.1088/1741-4326/ab2473>.
- [23] W. W. Heidbrink, J. Kim, and R. J. Groebner, Nucl. Fusion **28**, 1897 (1988).
- [24] R. B. White and M. S. Chance, Phys. Fluids **27**, 2455 (1984).
- [25] M. Gobbin, L. Marrelli, H. U. Fahrback, M. Garcia-Munoz, S. Gunter, P. Martin, R. B. White, and the ASDEX Upgrade Team, Nucl. Fusion **29**, 095021 (2009).
- [26] D. Terranova, T. Bolzonella, S. Cappello, P. Innocente, L. Marrelli, and R. Pasqualotto, Plasma Phys. Control Fusion **42**, 843 (2000).